LAWRENCE
LIVERMORE
NATIONAL
LABORATORY

UCRL-CONF-200447

A neutron sensor based on synthetic single crystal diamond

G. J. Schmid, N. Izumi, M. J. Moran, J. A. Koch, T. W. Phillips

October 21, 2003

A neutron sensor based on synthetic single crystal diamond
Albuquerque, NM, United States
October 27, 2003 through October 28, 2003

A neutron sensor based on single crystal CVD diamond

G.J. Schmid*, J.A. Koch, R.A. Lerche, M.J. Moran

University of California, Lawrence Livermore National Laboratory, Livermore , CA 94550

Abstract

We report the first neutron data for a single crystal Chemical Vapor Deposition (CVD) diamond sensor. Results are presented for 2.5, 14.1, and 14.9 MeV incident neutrons. We show that the energy resolution for 14.1 MeV neutrons is at least 2.9% (as limited by the energy spread of the incident neutrons), and perhaps as good as 0.4% (as extrapolated from high resolution α particle data). This result could be relevant to fusion neutron spectroscopy at machines like the International Thermonuclear Experimental Reactor (ITER). We also show that our sensor has a high neutron linear attenuation coefficient, due to the high atomic density of diamond, and this could lead to applications in fission neutron detection.

PACS: 29.40 *Keywords:* Radiation detector; single crystal CVD diamond; fusion neutron spectroscopy; ITER; fission neutron detection; alpha particle spectroscopy.

* Corresponding author. Address for correspondence: L-479, Lawrence Livermore National Laboratory, University of California, Livermore, CA 94550. Phone: 925-423-7866. Fax: 925-423-5517. E-mail: schmid3@llnl.gov

I. Introduction

Recent progress[1,2] in the growth of high purity single crystal CVD diamond has been quite dramatic. For example, some of the samples of Isberg et al[1] have shown charge collection distances greater than 10cm at 1V/μm, a figure that is orders of magnitude better than polycrystalline CVD diamond[3], and is representative of true "spectroscopic grade" material. This breakthrough opens the door to high resolution radiation sensors based on synthetic diamond.

Radiation sensors based on spectroscopic grade diamond have many potential applications. For example, high resolution, radiation hard, neutron spectrometers are needed for 14 MeV deuterium-tritium fusion machines like the International Thermonuclear Experimental Reactor (ITER)[4-5] and also the National Ignition Facility (NIF)[6-7]. While natural diamond gemstones[8-9] have already demonstrated energy resolutions approaching 2% at 14 MeV, synthetic single crystal CVD diamond offers the prospect of even better energy resolution due to higher purity and superior electrical properties. In addition, with the recent progress in the heteroepitaxial growth of single crystal CVD diamond[10-12], it is conceivable that large wafers could someday be available, perhaps comparable in size to the large silicon wafers of today. Assuming high electrical quality, these wafers would be useful not only for other neutron sensing applications (e.g. fast neutron radiography, fission neutron sensing) but also for x-ray and γ-ray sensing applications. In particular, since diamond actually has a higher electron density than silicon, but a lower K-edge, it could be useful as a front element in Compton scattering devices such as γ ray cameras[13] and γ ray polarimeters.[14]

The proposed application to fission neutron sensing is interesting enough to consider in a bit more detail. In Table I we list our calculated estimates of the linear attenuation coefficients for some promising fission neutron sensing materials at room temperature. The linear attenuation coefficient is equivalent to the intrinsic efficiency per unit thickness for zero energy threshold. According to these calculations, diamond appears to have the highest intrinsic efficiency for fission neutron detection per unit thickness, and hence per unit volume. This conclusion seems to hold true for arbitrary shape of the fission neutron spectrum (e.g. 1<T<2 MeV). Although cubic boron nitride (c-BN) is a close second, its electrical properties are relatively poor,[16] and the growth techniques are not well established[17], so it is not clear if practical radiation sensing will ever be possible with c-BN. Single crystal CVD diamond, on the other hand, can already be fabricated with very high electrical quality[1], and has the potential for extrapolation to large size[10]. If the wafers can be made large enough, some applications in fissile material detection could become possible.

In order to investigate single crystal CVD diamond as a neutron sensor, we have acquired a 3.0 x 3.0 x 0.5 mm wafer of Ultra-High Purity (UHP) single crystal CVD diamond from the same company that produced the Isberg[1] material (a company now known as Element Six, but formerly known as the DeBeers Industrial Diamond Division). We have used this wafer to construct the first neutron sensor based on single crystal CVD diamond, and have performed measurements at 2.5, 14.1 and 14.9 MeV. High resolution data acquired with α particles, x rays, and γ rays are also presented.

II. Experimental set-up

The present detector was fabricated by evaporating Ti-Pt-Au electrodes on either side of an intrinsic 3mm x 3mm x 0.5mm wafer of homoepitaxially grown single crystal CVD diamond[1]. The thickness of the electrode layers was nominally 100/200/1000 nm respectively. The unexposed edges of the wafer were subjected to an oxygen plasma treatment, and this generated a highly insulating device ($>10^{12}$ Ω at 100 V bias). The finished wafer was inserted into an Al housing structure, whereby one side of the wafer was grounded through contact with the inner side of the housing, and the other side was held in place by the conducting pin of a modified BNC connector. Typically, +100 V bias was applied across the wafer.

A schematic of the experimental set up is shown in Figure 1. Current pulses in the diamond sensor are generated when incident radiation produces electron-hole pairs in the bulk. This occurs via either collisions with valence electrons, in the case of incident charged particles or photons, or via knock-on ^{12}C nuclei or nuclear reaction products, in the case of incident neutrons. The current pulse, generated by the motion of the electrons and holes in the applied field, is integrated by a charge sensitive preamplifier (Ortec 142A). The resulting voltage pulseshape is amplified and shaped (0.5 μs shaping time) before digitization in an Analog-to-Digital Converter (ADC). The digitized signals, when histogrammed in a Multi-Channel Analyzer (MCA), produce a spectrum. The lower energy threshold in these spectra is set by the electromagnetic (EM) noise floor of the preamplifier (~14 keV).

III. Calibration with alpha particles

The diamond sensor was calibrated in vacuum using the 5.5 MeV α particles from a ^{241}Am source (Figures 2-5). Irradiation took place through the grounded Ti-Pt-Au electrode via a 1.5 mm hole in the center of the Al housing face. The average α particle count rate in the diamond was 1.2 counts/second. Since the range of the α particles in diamond is very short (~12μm), the signal is generated almost entirely by one carrier species (i.e. for positive bias, electron transport generates the signal, while for negative bias, hole transport generates the signal). By analysing the signal height vs. bias, it is possible to determine the μτ product for electrons and holes by way of the relation $\mu\tau = d/E$, where μ is the carrier mobility, τ is the mean carrier lifetime, d is the mean charge collection distance, and E is the applied electric field. Looking at Figure 2b, and recognizing that d is equal to the wafer thickness (0.5mm) at 63% total signal height, we can estimate that E = 66 V/mm for electrons and –20 V/mm for holes. The deduced μτ product is shown in Table II. The 10% error is from bias uncertainty.

The mobilities can be determined from the carrier transit times for a given bias. In principle, the transit time can be obtained from the risetime of the preamplifier pulseshape. Figure 3 shows that the intrinsic 5-95% risetime of our preamplifier is 12 ns. Figure 4a shows an α particle risetime test with a 1mm thick silicon surface barrier detector (Ortec) biased at 120V. The 5-95% risetime of this pulse is 60 ns. If we equate the risetime with the carrier transit time (t), we can determine the electron mobility (μ) through the relation $\mu = L/(Et)$, where L is the wafer thickness, and E=V/L. The result is 1390 cm^2/Vs, a value that agrees very well with the known electron mobility in silicon at room temperature (1350 cm^2/Vs).[15] The α particle pulseshapes for single crystal CVD diamond are shown in

Figures 4b and 4c. For +30V bias, the 5-95% risetime is 44 ns, while for –20V bias, the 5-95% risetime is 48 ns. Using the $\mu = L/(Et)$ relationship with L=0.5 mm, we get the mobility results shown in Table II. The 20% error estimates the uncertainty in equating the 5-95% risetime with the actual carrier transit time. By dividing the $\mu\tau$ result by the μ result, we get τ as shown in Table II.

The energy resolution of the diamond sample to incident α particles can be determined by taking the measured FWHM for the peak (68.4 keV from Figure 5), and subtracting (in quadrature) the FWHM for: energy straggling through the Ti-Pt-Au electrode (58.8 keV, shown in Figure 5); the intrinsic energy width of the ^{241}Am source (18 keV, from measurements with a Si surface barrier detector); and the electronic noise (14 keV, which can be extracted from the high side of the peak in Figure 8a). The net result is an energy resolution of 27 keV FWHM at E_α= 4.95 MeV (the mean energy of the α particles after transmission through the electrode) with 7 keV error. The error on this figure is dominated by uncertainties in the electrode thickness. In particular, although the nominal electrode thickness is 1.3μm, our own measurements, obtained by measuring the energy change of transmitted α particles when small amounts of the electrode are removed, indicate that the actual thickness is 12% less. This changes the energy straggling FWHM from 61.4 keV to 58.8 keV, and changes the ultimate resolution from 20 to 27 keV FWHM, and hence the quoted 7 keV error.

The mean energy required to create an electron hole pair (referred to as the ionization energy, ε) can be determined by comparing the α peak location in a diamond spectrum to either a calibrated pulser (Figure 6a) or to a silicon surface barrier detector (Figure 6b). In the case of the calibrated pulser (the BNC Model BH-1 calibrated against a Tektronix TDS

684B 1 GHz digital oscilloscope), we supply a known voltage step into the preamp test input which then injects a charge $Q=CV_p=(1\ pF)V_p$ into the preamp input line (V_p is the voltage step seen as seen by the internal capacitor, C, inside the preamp test input). To properly determine V_p, we correctly take into account the output impedance of the pulser, and also the input impedances of the calibrating scope and preamp. Once the value of V_p, and hence Q, is known, we can then calculate ε as $(1.6x10^{-19})E_\alpha/(.93Q)$, where the 0.93 factor corrects for the slightly different channel number between the pulser and α peaks in Figure 6a. The result is ε=13.2 eV. We can also compare directly to the silicon peak location in Figure 6b (knowing that silicon has ε=3.6 eV at room temperature), but we must correct for the fact that E_α is 10% higher at the silicon-electrode interface, as compared with the diamond-electrode interface, due to a much thinner electrode on the silicon. The final result is 13.9 eV. Averaging the above two results, we get 13.6 eV plus or minus 0.4 eV. This figure differs from the Japanese result[2] of 16.1 eV, but is in good agreement with previous studies of natural diamond gemstones[19].

One effect noted during the α particle tests was a degradation of signal height during extended irradiation times under positive bias. This effect, which was only noticed after 10 hours of continuous α irradiation at +100 V bias, and only for positive bias (not negative bias), would seem to indicate the presence of an electron trapping phenomenon. If trapped charge builds up in the volume, or on the surface, it lowers the bias inside the bulk, and thus results in lower signal height. By cycling the bias (i.e. turning the bias off and then on again), it has been noticed that the trapped charge disappears, and that normal operation can be restored. The exact mechanism for charge build up is not yet identified,

but can be speculated to be either carrier trapping in the diamond bulk (via impurities or lattice dislocations), or trapping at the electrode Schottky barrier.[20]

IV. Neutron measurements

Figures 7 shows the spectra produced by the diamond sensor for 2.5, 14.1 and 14.9 MeV incident neutrons. A maximum bias of 100 V was chosen to avoid surface breakdown of the diamond wafer (since neutron irradiation is a volume excitation, the sign of the bias should be unimportant). Neutrons were generated by a 150 kV deuteron beam striking either a deuterated (for 2.5 MeV) or tritiated (for ~14 MeV) target. The target was 1.4 cm diameter, and was at 45 degrees with respect to the beam direction. The detector, located between 2 and 3 cm from the target, was at 90 degrees with respect to the beam for the studies at 2.5 and 14.1 MeV, but was shifted to 0 degrees to acquire 14.9 MeV neutron data. The shape of the 2.5 MeV spectrum (Figure 7a) is determined by the features of the elastic scattering differential cross section. At 14.1 and 14.9 MeV, the shape is due to a combination of elastic scattering, inelastic scattering, and (n,α) reactions, as discussed theoretically by Pillon[8]. The peak on the far right-hand side of the 14.1 MeV spectrum, which represents 8.4 MeV energy deposition, is due to the (n,α) reactions in diamond which lead to the ground state of ^{9}Be. The finite geometry of the experiment leads to a large energy spread of the incident neutrons, and this entirely determines the 240 keV FWHM width of the (n,α) peak in Figure 7b (as determined by Monte Carlo simulation of the kinematics and geometry). The intrinsic width of the diamond sensor to 14.1 MeV neutrons can be estimated from the α particle data (via the $E^{-1/2}$ scaling law[15]) to be ~35 keV FWHM. Figure 7c shows that the peak location depends sensitively on neutron energy ($E_{peak} = E_n - 5.7$ MeV), and demonstrates the potential for accurate neutron

spectroscopy. While this effect has already been noted for natural diamond gemstones[8], we report it here for synthetic diamond for the first time.

Based on the diamond neutron data, along with the total neutron yields as acquired via associated particle counting, it is possible to extract experimental values for the efficiency per unit thickness, and to compare this to calculation. For our diamond sensor, the experimental values at 2.5 and 14 MeV are 2.2 and 2.4 %/mm respectively (with an approximate error of +/– 0.3 %/mm). The experimental thresholds were ~20-30 keV (estimated carbon recoil energy). These experimental efficiency numbers are in reasonable agreement with the calculated zero energy threshold efficiency values of 2.7 and 2.3 %/mm (for 2.5 and 14 MeV neutrons respectively). This lends some credence to the zero energy threshold calculations (i.e. μ_n) presented in Table I. However, for the heavier elements in Table I, whereby a smaller energy transfer takes place in the neutron scattering, and also for the scintillators, in which the carbon atoms are known to be less efficient at producing light than the recoil hydrogen atoms[15], the pulse height will be low, and thus the calculations will tend to be overoptimistic as compared with real world measurements. For example, we undertook a measurement at 2.5 MeV with a BC400 plastic scintillator (from Bicron), and found a neutron efficiency per unit thickness of 0.9 %/mm at ~20 keV threshold (estimated proton recoil energy). This is less than half of the zero energy threshold calculated value of 2.2 %/mm at 2.5 MeV, and indicates that the carbon atoms are probably not producing any measurable light yield.

V. X-ray/γ ray measurements

Measurements with x rays and γ rays were also performed, and are shown in Figure 8. In these tests, the x rays were incident from the front, but the γ rays were incident from the side in order to optimise collection of the Compton backscattered electrons.

VI. Conclusions

In summary, we have taken the first neutron data with a single crystal CVD diamond radiation sensor. The results at 14.1 MeV demonstrate a quality that is "spectroscopic grade". In particular, the energy resolution for the 8.4 MeV (n,α) peak is shown to be at least 2.9% (i.e. 240 keV FWHM), as limited by the spread of the incident neutrons, and perhaps as good as 0.4% (i.e. 35 keV FWHM) if the extrapolation with α particle data is to be trusted. Measurements with x rays and γ rays have also been presented. Furthermore, we have shown theoretically that diamond has a high linear attenuation coefficient for fission neutrons: perhaps higher than any other room temperature sensor material. This could translate into the highest efficiency per unit volume for fission neutron sensing. As such, if large, high quality, wafers of single crystal CVD diamond could be synthesized, they might be useful in some scenarios for the detection of fissile materials. Such large wafers could also be advantageously applied to other areas of radiation sensing, as has been discussed.

Further studies with single crystal CVD diamond neutron sensors are now suggested. Of primary interest would the verification of the 35 keV FWHM predicted energy resolution to monoenergetic 14 MeV neutrons. Obtaining truly monoenergetic 14 MeV neutrons would be difficult, but could possibly be accomplished with a high yield DT

neutron generator and a detector that is placed far away from the target at the precise angle of 98 degrees[21] with respect to the beam direction. If the intrinsic resolution, as measured in this fashion, turns out to be higher than 35 keV FWHM, it could indicate a here-to-fore unrecognised phenomenon in diamond. In particular, it may be that the diamond response to the α and ^{9}Be particles in the (n,α) exit channel is slightly different, and that the kinematic-dependent energy sharing between these two causes an extra broadening in the peak. Accelerator based studies using MeV beams of α and ^{9}Be nuclei could help clear up this issue. Another area of further study would be to undertake fission neutron measurements with single crystal CVD diamond, and to compare to other materials, and also to the theoretical results of Table I.

Acknowledgements We thank N. Izumi, N. Madden and E. Hull for helpful discussions, A. Friensehner and M. Fowler for detector manufacture, G. Mant for experimental set up, and W. Farmer for data acquisition. The diamond wafers used in this work were manufactured by Element Six and were purchased by us through Harris International, NY. This work was performed at the University of California, Lawrence Livermore National Laboratory, under the auspices of the US Department of Energy under contract W-7405-Eng-48.

References

1. Isberg, J. *et al. Science* **297,** 1670-1672 (2002).

2. Kaneko, J.H. *et al*. *Nuclear Instruments and Methods in Physics Research, Section A* **505**,187-190 (2003)

3. Hrubec J, *et al. Nuclear Instruments and Methods in Physics Research Section A* **434**, 131-145 (1999)

4. Aymar, R. *Fusion Engineering and Design* **55**, 107-118 (2001)

5. Johnson , L.C. *et al*. *Review of Scientific Instruments* **68**, 569-72 (1997)

6. Moses, E.I., Wuest, C.R. *Fusion Science and Technology* **43**, 420-427 (2003)

7. Murphy, T.J. *et al. Review of Scientific Instruments* **72**, 773-9 (2001)

8. Pillon, M., Angelone, M.., Krasilnikov, A.V. *Nuclear Instruments and Methods in Physics Research, Section B***101**, 473-483 (1995)

9. Isobe, M. *et al*. *Fusion Engineering & Design* **34-35**, 573-6 (1997).

10. Lee, S.T., Lifshitz, Y. *Nature* **424**, 500-501 (2003)

11. Dai, Z., Bednarski-Meinke C., Loloee, R., Golding, B. *Applied Physics Letters* **82**, 3847-3849 (2003)

12. Bednarski, C. Dai, Z., Li, A.-P. *Diamond and Related Materials* **12**, 241-245 (2003)

13. Tomitani, T., Hirasawa, M. *Physics in Medicine and Biology.* **47**, 2129-45 (2002)

14. Coburn, W., Boggs, S.E. *Nature* **423**, 415-417 (2003)

15. Knoll, G.F. *Radiation Detection and Measurement* (JWS, New York, 2000)

16. Mohammad, S.N. *Solid-State Electronics* **46**, 203-222 (2002)

17. Bello, I. *et al. in Proceedings of the 4th International Conference on Advanced Semiconductor Devices and Microsystems (ASDAM 2002)*, Slovakia, p.1-11 (2002)

18. Ziegler, J.F., Biersck, J.P. *The stopping and range of ions in solids* (Pergammon Press, New York, 1985)

19. Canali, C. *et al. Nuclear Instruments and Methods* **160**, 73-77 (1979)

20. Rhoderick, E.H. *Metal-semiconductor contacts.* (Clarendon Press, Oxford, 1978)

21. Seagrave, J.D. *et al.* D(d,n)He^3 and T(d,n)He^4 neutron source handbook. *Los Alamos National Laboratory internal report.* LAMS-2162 (1957)

Table I: Room temperature sensor materials for fission neutron detection

Material	n (atoms/cm^3)	$\langle\sigma_n\rangle$(b)†	$\langle\mu_n\rangle$ (%/mm)††
Diamond	17.6×10^{22}	2.31	4.1
c-BN	17.3×10^{22}	2.16	3.7
BC517p*	11.1×10^{22}	3.19	3.5
BC400**	10.0×10^{22}	3.00	3.0
SiC	9.6×10^{22}	2.65	2.5
GaN	8.8×10^{22}	2.85	2.5
ZnO	8.3×10^{22}	3.49	2.9
GaAs	4.4×10^{22}	4.17	1.8

†Cross sections averaged over an unmoderated spontaneous fission neutron spectrum[15] with a T parameter of 1.6 MeV (the cross section data is from the ENDL database, http://www-ndg.llnl.gov/).
††The linear attenuation coefficient for incident neutrons averaged over the same fission spectrum.
*Liquid scintillator[15]. **Plastic scintillator[15].

Table II: Carrier mobility (μ) and lifetime (τ) as derived from α particle data

	μτ (cm^2/V)	μ (cm^2/Vs)	τ (ns)
electrons	1.2×10^{-4}	1.9×10^{3}	60
holes	7.1×10^{-4}	2.6×10^{3}	270
Approx. error	+/- 10%	+/- 20%	+/- 25%

Figure 1: The single crystal CVD diamond wafer (shaded) is secured in a 2-piece Al housing structure (on left) which is held together by a set screw. One side of the wafer presses against the Al housing surface (gnd) and the other side is held in place by the modified pin of a BNC connector. The BNC connects to an ORTEC 142A preamplifier which supplies the detector bias (e.g. +100 V). The rest of the electronic processing chain is also shown.

Figure 2: a) Single crystal CVD diamond sensor α particle spectra from a ^{241}Am source showing improvement compared to a 0.5mm thick, radiation pumped, e-grade, polycrystalline CVD diamond sensor (akin to those in ref.3), whereby the single crystal diamond is biased at +100 V, and the polycrystalline diamond is biased at the peak-height saturated level of +200 V; b) peak channel number vs. bias for ^{241}Am α particles into the single crystal CVD diamond sensor (for negative bias, input polarity of amplifier is switched).

Figure 3: a) Step pulse of a BNC Model BH-1 Pulser as recorded with a 1GHz Tektronix TDS digital oscilloscope; b) Pulseshape from the Ortec 142A preamplifier with the pulser signal placed into the test input. The dotted lines are the actual recorded data, while the superimposed solid lines are the smoothed pulseshapes used for analysis. The 5-95% risetimes, which are 16 and 20 ns respectively, are determined using a high level extracted well to the right of the transition region (as recommended in the Ortec manual). If we subtract the two risetimes in quadrature, we obtain an intrinsic preamp + cable risetime of 12 ns.

Figure 4: Preamplifier pulseshapes for ^{241}Am α particles injected into the: a) Silicon surface barrier detector, 1mm thick, biased at +120 V; b) Single crystal

CVD diamond sensor biased at +30 V; c) Single crystal CVD diamond sensor biased at –20V.

Figure 5: A high statistics measurement of the ^{241}Am α particle lineshape in the single crystal CVD diamond sensor (solid line). Bias is –100 V, but with different amplifier settings than figure 2. The FWHM of this lineshape is 68.4 keV, and is dominated by the energy straggling of the incident α particles through the Ti-Pt-Au electrode. This contribution is 58.8 keV FWHM, and is determined by a TRIM[18] Monte Carlo simulation (dotted line). The tail on the low side of the measured peak is due to a small satellite ^{241}Am peak that is not included in the TRIM simulation.

Figure 6: Calibration of the single crystal CVD diamond sensor can be accomplished by comparing the ^{241}Am α particle peak position with: a) Injection of 6.5 x 10^{-14} C into the preamp via a pulser; b) an α spectrum from an Ortec silicon surface barrier detector (assuming one corrects for the 10% higher α energy in the silicon due to a thinner electrode). The diamond peak shown above is for +160 V bias, but with different amplifier settings than previous figures.

Figure 7: Counts vs. energy deposited in single crystal CVD diamond sensor for incident neutrons of energy a) 2.5 MeV, b) 14.1 MeV, and c) 14.1 and 14.9 MeV (expanded view showing the (n,α) peaks). The spectra have been calibrated based on known endpoint energies: 700 keV for the 2.5 MeV neutrons, and 8.4 MeV for the 14.1 MeV neutrons. All data at +100 V bias.

Figure 8: Counts vs. energy deposited in single crystal CVD diamond sensor for incident photons of energy a) 22 keV (the x rays from ^{109}Cd), and b) 662 keV (the γ

rays from ^{137}Cs). The top plot is calibrated with the 22 keV photopeak, while the bottom plot is calibrated with the Compton backscattered edge (478 keV). All data at +100 V bias.

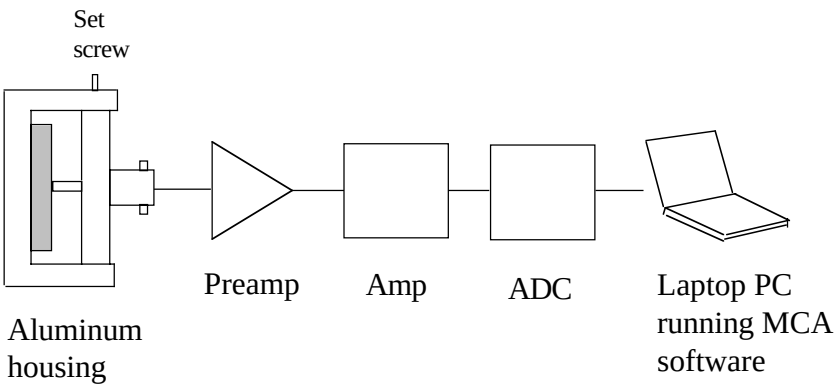
Set
screw
Preamp
Amp
ADC
Laptop PC
running MCA
software
Aluminum
housing

Figure 1

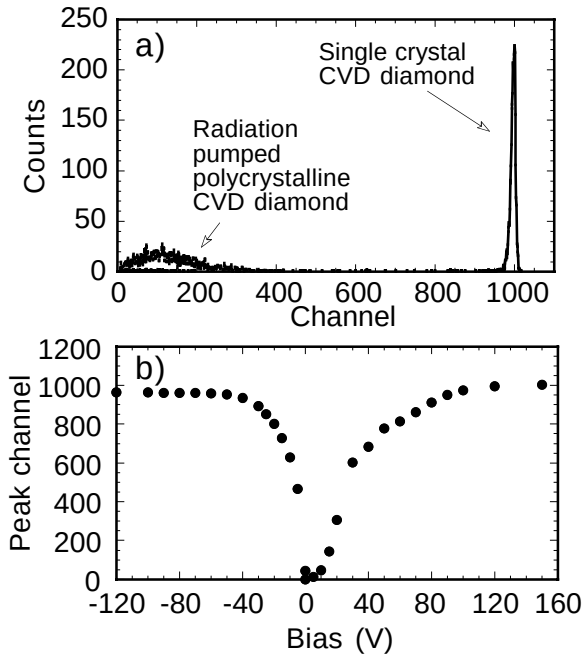
a)
Single crystal
CVD diamond
Radiation
pumped
polycrystalline
CVD diamond
Counts
Channel
b)
Peak channel
Bias (V)

Figure 2

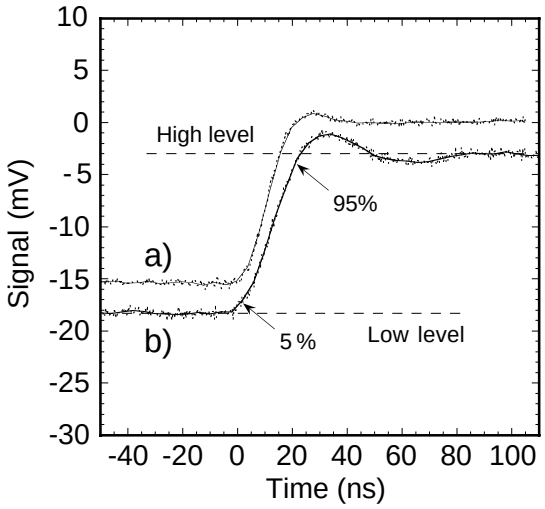
10
5
0
-5
-10
-15
-20
-25
-30
Signal (mV)
-40 -20 0 20 40 60 80 100
Time (ns)
High level
95%
a)
b)
5 %
Low level

Figure 3

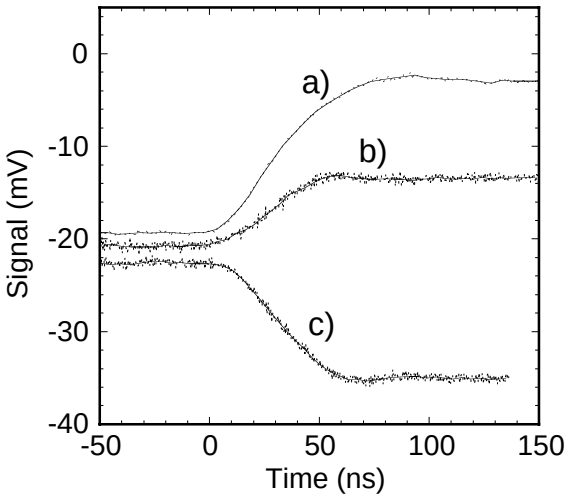

Figure 4

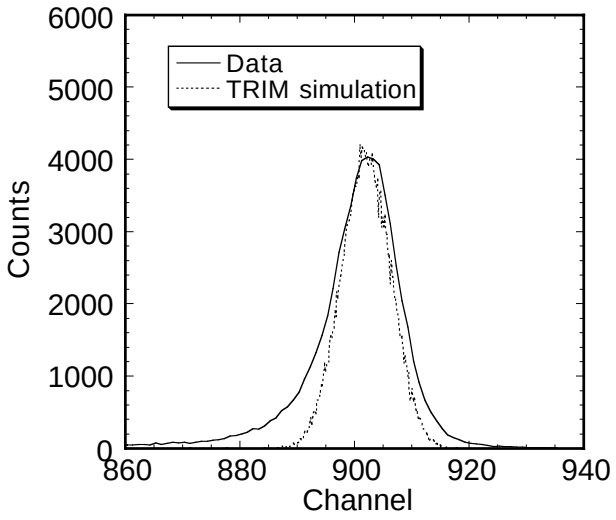
6000
5000
4000
3000
2000
1000
0
Counts
860
880
900
920
940
Channel
Data
TRIM simulation

Figure 5

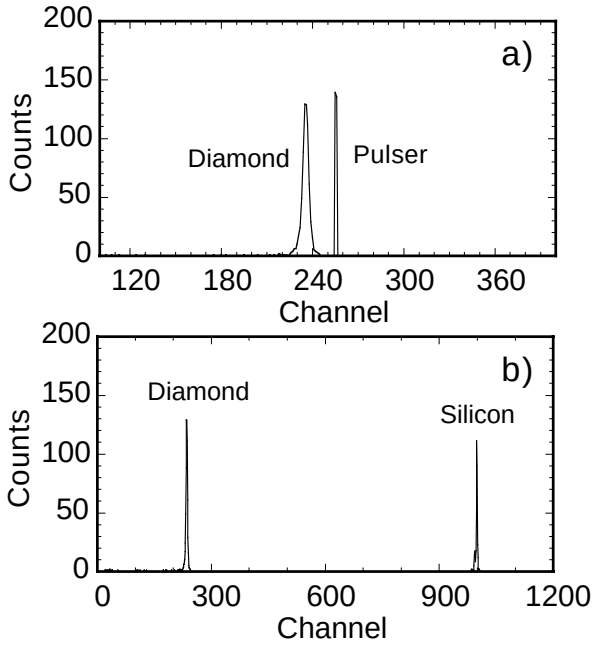
a)
Diamond
Pulser
Counts
Channel
b)
Diamond
Silicon
Counts
Channel

Figure 6

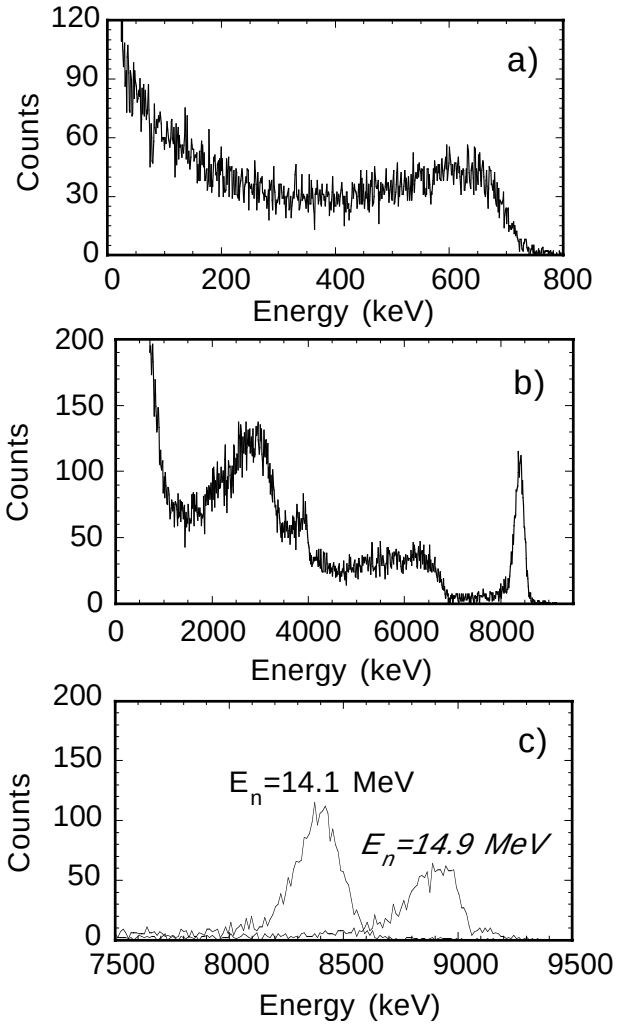
a)
Counts
Energy (keV)
b)
Counts
Energy (keV)
c)
E_n=14.1 MeV
E_n=14.9 MeV
Counts
Energy (keV)

Figure 7

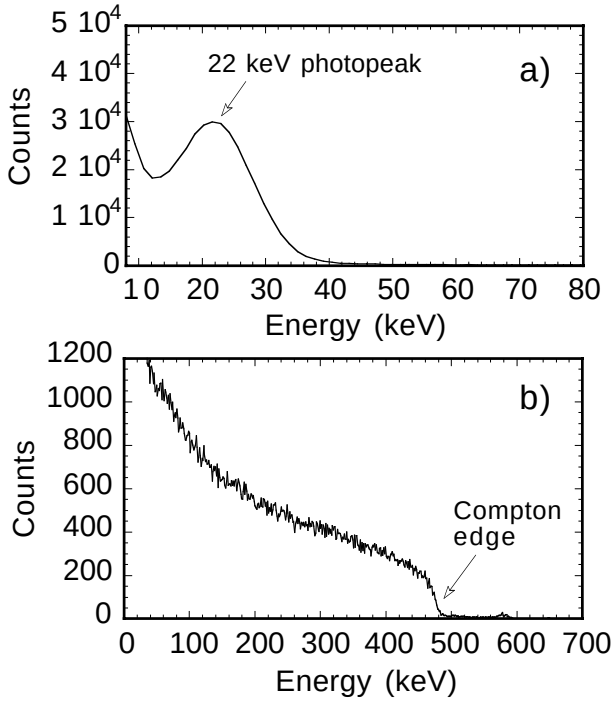
5 10^4
4 10^4
3 10^4
2 10^4
1 10^4
0
Counts
22 keV photopeak
a)
10 20 30 40 50 60 70 80
Energy (keV)
1200
1000
800
600
400
200
0
Counts
b)
Compton
edge
0 100 200 300 400 500 600 700
Energy (keV)

Figure 8